AIP | Journal of Applied Physics

Multiphonon scattering and photoluminescence of two dimensional ZnS nanosheets grown within Na-4 mica

Amrita Mandal, Sreemanta Mitra, Anindya Datta, Sourish Banerjee, Sandip Dhara et al.

Citation: J. Appl. Phys. **112**, 074321 (2012); doi: 10.1063/1.4757930
View online: http://dx.doi.org/10.1063/1.4757930
View Table of Contents: http://jap.aip.org/resource/1/JAPIAU/v112/i7
Published by the AIP Publishing LLC.

Multiphonon scattering and photoluminescence of two dimensional ZnS nanosheets grown within Na-4 mica

Amrita Mandal,[1,2] Sreemanta Mitra,[1,2] Anindya Datta,[3] Sourish Banerjee,[2] Sandip Dhara,[4,a)] and Dipankar Chakravorty[1,a)]
[1]*MLS Professor's Unit, Indian Association for the Cultivation of Science, Jadavpur, Kolkata 700 032, India*
[2]*Department of Physics, University of Calcutta, Kolkata 700 009, India*
[3]*University School of Basic and Applied Science (USBAS), Guru Gobind Singh Indraprastha University, New Delhi, India*
[4]*Surface and Nanoscience Division, Indira Gandhi Centre for Atomic Research, Kalpakkam 603102, India*

(Received 29 June 2012; accepted 10 September 2012; published online 9 October 2012)

Two dimensional wurtzite ZnS nanosheets with thickness of 0.6 nm are grown within the interlayer spaces of sodium fluorophlogopite mica (Na-4 mica) using ion-exchange-cum-solution treatment method followed by sulfidation treatment at 873 K. The presence of wurtzite ZnS is confirmed by x-ray diffraction, electron microscopy, and Raman scattering studies. The two dimensional form of ZnS gives rise to a strong quantum confinement with the band gap blue shifted by 1.7 eV. Thickness of the nanosheet is confirmed using atomic force microscopy. Raman scattering studies show higher order transverse optical modes due to increased deformation potential in reduced dimension. In contrast to red shift of optical phonon modes in phonon confinement model, a blue shift observed is ascribed to a compressive stress on ZnS nanosheets grown within Na-4 mica interlayer spaces. An additional band at 315 cm^{-1} is assigned to surface optical phonon. Unusual broadening in room temperature photoluminescence spectrum may be due to strong coupling of excitons with overtones of longitudinal optical phonon modes. © *2012 American Institute of Physics*. [http://dx.doi.org/10.1063/1.4757930]

I. INTRODUCTION

ZnS is an important material within the family of wide band gap semiconductors owing to its novel properties and varieties of applications. This material is widely used in electroluminescent devices, light-emitting diodes, sensors, lasers, display systems, and solar cells.[1–5] ZnS is also an attractive candidate for its use in bio-imaging applications, due to its nonlinear multiphoton absorption characteristics in the visible to infrared range.[6,7] Nanocrystals of ZnS play more important role than their bulk counterparts because of improved physical properties owing to the electronic quantum confinement effect.[8,9] Enhanced thermoluminescence,[10] high quantum efficiency of the emission line, and very short luminescence decay times have been observed in ZnS nanocrystals.[11–13]

Blue shift of the absorption spectra, i.e., increase in band gap is one of the most interesting results of quantum confinement effect.[12] There are several reports on blue shift of band gap for ZnS with decreasing particle size. Li *et al.* showed blue shift of ~0.83 eV in case of ZnS quantum dots.[14] A blue shift of 0.86 eV was observed in case of hexagonal ZnS nanocrystals.[15] Sapra *et al.* have reported a large increase (~1.1 eV) in band gap, with decreasing cluster size, than that in the bulk.[16] Large band gap makes the semiconductors attractive for applications in the UV range. ZnS crystallizes in two basic structures of cubic zinc blende and hexagonal wurtzite.[17] Zinc blende is the most stable form at low temperatures. In the bulk form, ZnS transforms to wurtzite phase at temperatures higher than 1296 K.[18–20] This transition temperature is reduced to 673 K for nanoparticles.[20] High temperature vapor based synthesis has been used effectively to prepare a similar phase.[21] Solvothermal technique has been found to be also suitable to grow the hexagonal phase around 673 K temperature.[18] In the present report, we have achieved formation of a stable and pure wurtzite ZnS at 873 K by using a simple ion exchange-cum-solution treatment technique. Various nanostructures of ZnS have been reported so far. Most of them are essentially one dimensional (1D) and their hierarchical nanostructures.[22–30] However, only a few reports are available on two dimensional (2D) nanostructures.[19,31–33] Vapor based techniques such as thermal evaporation and chemical vapor deposition are well established to form anisotropic nanostructures such as nanobelts and nanosheets in a large scale.[21,32] But the thickness of nanostructures achieved by these methods is not less than 5 nm. In our experiment, we have been able to achieve ~0.6 nm thickness, however, not in a large scale but with uniform thickness for all nanosheets.

Although the synthesis procedure has already been established by our group,[34–36] but our objective is to explore this method to synthesize different materials and investigate the significant changes in their physical properties. In the present study, ultrathin nanosheets of ZnS with thickness ~0.6 nm have been synthesized within the interlayer spaces of Na-4 mica. The thickness was confirmed by atomic force microscopic (AFM) measurements. Pure hexagonal phase of ZnS was confirmed by x-ray diffraction studies (XRD), transmission

a)Authors to whom correspondence should be addressed. Electronic addresses: mlsdc@iacs.res.in and dhara@igcar.gov.in.

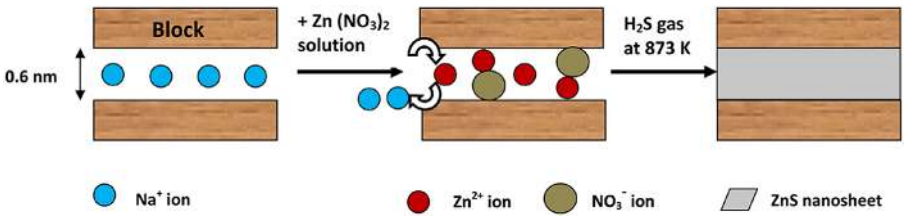

FIG. 1. Schematic representation of synthesis procedure.

electron microscopy (TEM), and Raman analysis. The nanosheets have exhibited a large increase in band gap which has not been reported so far. Also, the Raman spectra have showed some unusual features which could be ascribed to the 2D morphology of ZnS sheets. Our primary objective is to delineate the effect of two-dimensionality on the optical properties of wurtzite phase of ZnS.

II. EXPERIMENTAL

In the present work Na-4 mica ($Na_4Mg_6Al_4Si_4O_{20}F_4{\cdot}xH_2O$) was prepared first by sol-gel method, the details of which were reported earlier.[36,37] The Na-4 mica (powder) was immersed in a solution of $Zn(NO_3)_2$ in water for the ion exchange reaction which involved replacement of Na^+ ions in the mica structure by Zn^{2+} ions from $Zn(NO_3)_2$ solution. In this process Na^+ ions moved out of Na-4 mica and got into the initiate solution. The solution was kept inside an autoclave at 373 K for one week. Also the interlayer spaces got filled up by $Zn(NO_3)_2$ solution which provided both Zn^{2+} and $(NO_3)^-$ ions. Two Na^+ ions are replaced by one zinc ion Zn^{2+}. The treated powder was filtered and washed thoroughly with deionized water to remove excess nitrate salt. The powder was subjected to a sulfidation treatment in H_2S gas flow at 873 K for 1 h. ZnS was formed within the interlayer spaces of Na-4 mica. Formation of ZnS was effected from both Zn^{2+} ions exchanged with Na^+ ions as well as Zn^{2+} ions derived from the $Zn(NO_3)_2$ solution filling up the interlayer spaces. Synthesis procedure is represented schematically by Fig. 1.

XRD pattern of ZnS grown within Na-4 mica was recorded in BRUKER D8 XRD SWAX diffractometer using CuK_α radiation. For studying the microstructure, ZnS nanosheets were extracted from Na-4 mica by etching the composite sample with 10% HF aqueous solution and then centrifuging in SORVALL RC 90 ultracentrifuge at 30 000 rpm for 30 min. The etched sample was investigated by a JEOL Model JEM 2010 TEM. For AFM study the etching process was performed for a longer time to remove Na-4 mica phase completely. In this case, the nanocomposite powder was immersed in 10% HF aqueous solution for 4 days. A very little amount of this solution was added to acetone to make a dilute solution. The latter containing ZnS nanosheets were deposited on freshly cleaved atomically flat mica surface (SPI, USA), and the sample was investigated by Veeco model CP II AFM. The other measurements were carried out on unetched samples. Both Raman scattering and photoluminescence (PL) studies were performed with 325 nm (3.81 eV) excitation of continuous wave He-Cd laser and dispersion with 2400 gr/mm grating in the backscattering configuration using Raman spectrometer (inVia Renishaw). Raman scattering for excitations of 514.5 and 785 nm of Ar^+ laser and InGaAs laser, respectively, was also studied using dispersion with 1800 gr/mm gratings. A thermoelectric cooled "back-thinned" CCD detector was used for the detection of scattered intensity. The UV-VIS absorption spectrum was recorded in a Varian Cary 5000 UV-Vis-NIR spectrometer.

III. RESULTS AND DISCUSSION

As discussed previously, we have used Na-4 mica as a template to form 2D nanocrystals. It belongs to clay mineral group which has a layered structure consisting of blocks (made up of Al, Mg, Si, F, and O atoms) separated by an interlayer space of ~0.6 nm thickness. There are four Na^+ ions per unit cell within this interlayer space which are very weakly bound to oxygen ions of the upper and lower blocks. During ion exchange reaction, due to concentration gradient Zn^{2+} ions diffused inside the interlayer space and replaced Na^+ ions. To balance the charge two Na^+ ions were exchanged with one Zn^{2+} ion. $Zn(NO_3)_2$ solution also filled up the interlayer spaces of Na-4 mica structures, thus providing Zn^{2+} and $(NO_3)^-$ ions. The sulfidation treatment at proper temperature ultimately created two dimensional ZnS nanosheets confined within the interlayer spaces of Na-4 mica. The thickness of the interlayer spaces was estimated from interplanar spacing (d_{hkl}) values of (001) and (002) planes of Na-4 mica, where (001) is the basal plane of mica. The d_{hkl} values of (001) and (002) planes were reported to be 1.21 and 0.61 nm, respectively.[38] The thickness of the interlayer spaces (0.6 nm) was obtained by subtracting the d_{hkl} value of (002) plane from that of (001) plane. Figure 2 shows the XRD patterns of ZnS nanosheets grown within Na-4

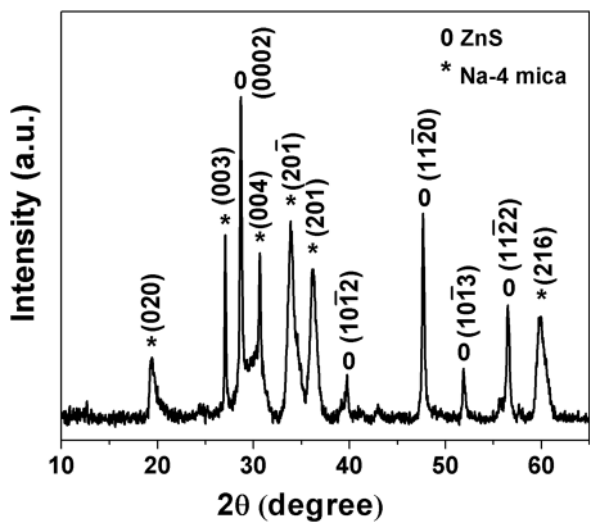

FIG. 2. X-ray diffactrogram of ZnS-mica nanocomposite.

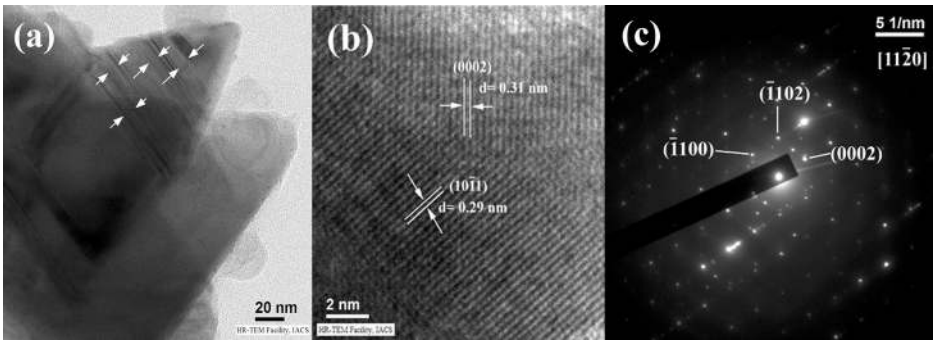

FIG. 3. (a) Transmission electron micrograph of ZnS nanosheets. Modulation on the surface is indicated by arrows. (b) High resolution lattice image of ZnS nanosheets from Fig. 2(a). (c) Selected area electron diffraction pattern of nanosheets.

mica template. The planes corresponding to both ZnS and Na-4 mica are indexed in this figure. The nanocomposite consists of wurtzite ZnS (JCPDS file: 75-1534) and monoclinic Na-4 mica phases,[39] respectively. The formation of ZnS nanosheet is also confirmed from the transmission electron micrographs of the etched samples. The images are shown in Figures 3(a)–3(c). Figure 3(a) shows triangular nanosheet like structures of ZnS. The arrows indicate surface roughness modulation which is discussed later. High-resolution lattice image [Fig. 3(b)] reveals the (10$\bar{1}$1) and (0002) planes of ZnS with interplanar spacings (d_{hkl}) of 0.29 and 0.31 nm, respectively. These values are in good agreement with those given in JCPDS file for hexagonal ZnS. The symmetry in the selected area electron diffraction pattern [Fig. 3(c)] recorded along [11$\bar{2}$0] zone axis indicates that nanosheets grow along its *c*-plane (perpendicular to *c*-axis). These planes should be parallel to the basal planes of Na-4 mica because the other dimension along *c*-axis of Na-4 mica is confined by the blocks as mentioned earlier. The XRD pattern also supports this view. In the diffraction pattern, the presence of (0002) plane of ZnS with maximum intensity along with (003) and (004) planes [family members of (001) basal plane] of Na-4 mica with comparable intensities indicate that the planes are parallel to each other.

The thickness of the nanosheets is confirmed by AFM study. Figure 4 shows a typical height profile obtained in the case of ZnS nanosheets deposited on atomically flat mica surface (as mentioned earlier) using an AFM. The measured height of a single nanosheet is 0.6 nm which confirms that the ZnS nanosheets indeed grew within the interlayer spaces (thickness $\sim$ 0.6 nm) of Na-4 mica structures. The lateral width of the single nanosheets is $\sim$50 nm which is quite less compared to the width of nanosheets shown in TEM image [Fig. 3(a)]. During the sample preparation for AFM study, the nanocomposites were etched for a longer time than that for TEM study. Therefore, some nanosheets may have been broken during this sample preparation process, and we have not been able to get the profile of a large sheet.

Electronic properties of low dimensional semiconductors depend on their dimensionality because their density of states varies with dimension. The density of state changes its nature from a continuous function to step-like nature from 3D to 2D system.[40] Therefore, optical properties are also influenced by the dimensions of the material and vary significantly from 0D to 1D and 2D materials. Recently, Schliehe's group has reported the effect of confinement in case of ultrathin PbS sheets, which are confined only in vertical direction.[41] They showed that the emission for nanosheets was blue shifted by $\sim$70 nm compared to that of PbS quantum dots. Figure 5 shows the UV-Vis absorption spectrum of ZnS-Na-4 mica system at room temperature. We found two broad peaks at 227 and 336 nm, respectively. The optical absorption spectrum of an ideal 2D system is step-like in nature.[40] In our experiment, we have dispersed powdered sample in ethanol for optical studies, where the 2D nanosheets are randomly oriented. Therefore it has not been possible to get an ideal 2D system; however, the UV-Vis spectrum shows a slight step-like trend (as indicated by the arrows). The two broad peaks are believed to arise due to the two dimensional nature of ZnS nanosheets. The nanosheets are strongly confined in one direction, whereas there are no confinements in other two directions. Because of the random alignments and natural agglomeration of the nanosheets there will be a pseudo three-dimensional configuration of the material which will prevail during the absorption measurements. This explains the observation of the peak at 336 nm corresponding to the band gap value of bulk ZnS (3.7 eV).[42] The quantum confinement effect will be observed, however, for some of the nanosheets having an alignment perpendicular to the incident radiation. This will explain the appearance of the absorption peak at 227 nm (5.4 eV). The optical band gap was determined using the following formula[42] for direct interband transitions:

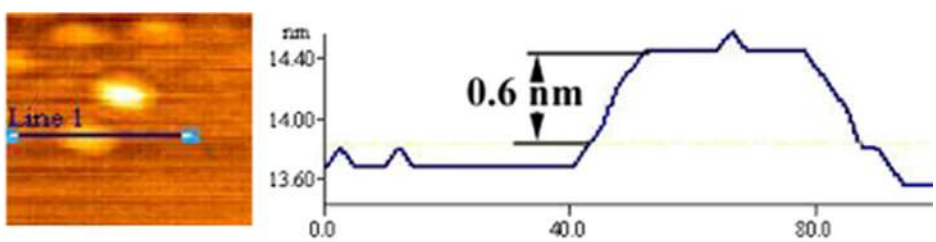

FIG. 4. AFM image and the height profile of ZnS nanosheet.

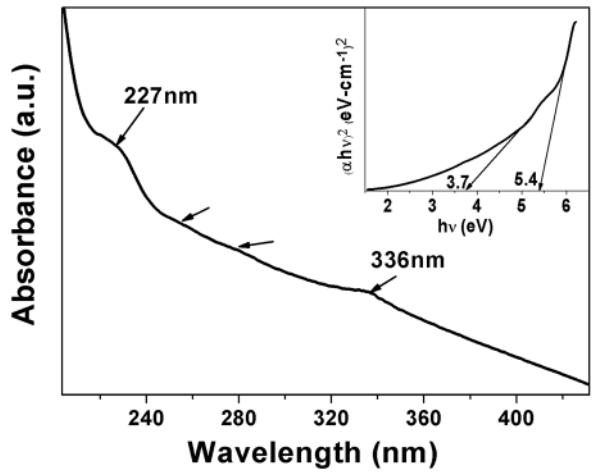

FIG. 5. UV-vis absorption spectrum of ZnS-mica nanocomposite. (inset) Plot of $(\alpha h\nu)^2$ vs $h\nu$.

$$(\alpha h\nu)^2 = A(h\nu - E_g), \tag{1}$$

where A is a constant, $h\nu$ is the incident photon energy, E_g is optical band gap, and α is absorption coefficient. Hence, the optical band gap can be obtained by extrapolating the linear portion of the plot $(\alpha h\nu)^2$ vs $h\nu$ to $\alpha = 0$ in the inset of Figure 5. E_g was found to be 5.4 eV, corresponding to the peak at 227 nm and thus was blue shifted by 1.7 eV from that of bulk ZnS (3.7 eV) due to the effect of quantum confinement.[42] Such a large blue shift was previously reported for cubic ZnS nanoparticles,[43,44] whereas for wurtzite ZnS nanocrystals the maximum band gap reported earlier was 4.77 eV.[16] Considering this band gap shift, the thickness of the nanosheet was estimated using the following relation:[45]

$$\Delta E_g = \frac{\pi^2\hbar^2}{2\mu L_z^2}, \tag{2}$$

where ΔE_g is band gap shift, L_z is the film thickness, and μ is the reduced electron-hole effective mass of ZnS

$$\frac{1}{\mu} = \frac{1}{m_e} + \frac{1}{m_h}, \tag{3}$$

and m_e and m_h are the electron and hole effective masses, respectively. Considering $m_e = 0.42m_0$ and $m_h = 0.61m_0$,[19] with m_0 being the electron rest mass, the thickness of nanosheet was found to be 0.9 nm for 1.7 eV band gap shift. Considering the approximation used in calculating the values of the effective masses and the rather wide variation being reported in the literature,[46] the estimated thickness value is reasonable, as estimated from the crystallographic consideration for the growth of ZnS after sulfidation. The stacking layers of mica provide a confined space of ~0.6 nm for the growth of 2-D ZnS films, which is barely wide enough to create just a few layers of ZnS ($c = 0.6527$ nm).[47] Another peak at 336 nm (Fig. 5) corresponds to $\alpha = 0$ at 3.7 eV (inset of Fig. 5) which indicates the band gap value of bulk ZnS (3.7 eV). Therefore, the absorption spectrum covers a wide range of wavelength with two absorption peaks within UV-C (~200–290 nm) and UV-A (~320–400 nm) regions. Thus,

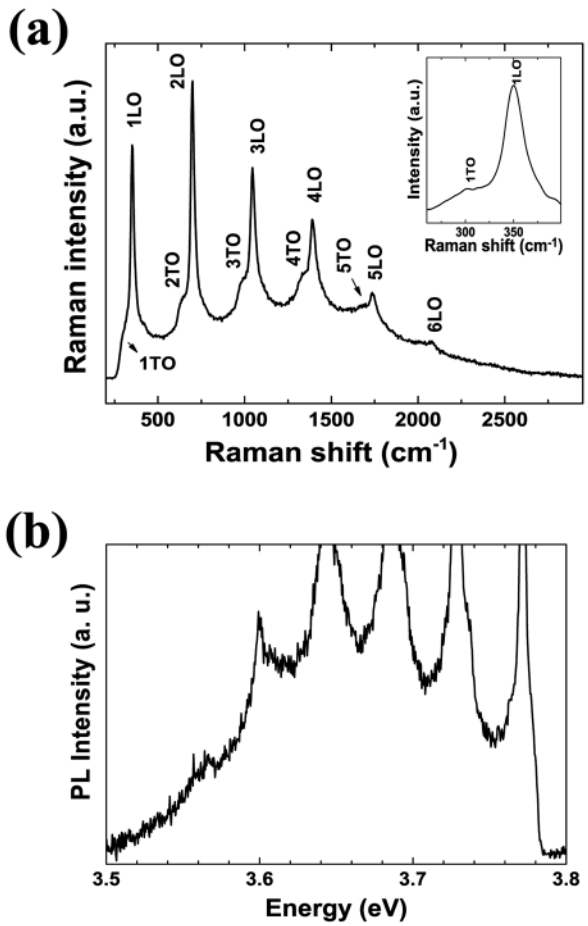

FIG. 6. (a) Multiphonon resonance Raman modes showing higher order LO and TO modes of wurtite ZnS using 3.81 eV excitation. Inset shows the first order modes. (b) PL spectrum of ZnS-mica nanocomposite at room temperature.

the nanocomposite can be used as a detector for both UV-C as well as UV-A band. A rather long tail in the absorption spectra is noteworthy. Though a satisfactory explanation is not available at present, it is probable that there is a smearing out of a number of steps due to a 2D structure (as mentioned above) which leads to this result. This effect has been observed, as pointed out earlier, within the wavelength range 227 and 336 nm.

Figure 6(a) shows the multiphonon resonance Raman scattering studies using 3.81 eV excitation for longitudinal and transverse optical (LO and TO) modes along with first order modes in the inset for clear identification of LO and TO mode peak positions. Mode frequency values of ~300 cm^{-1} and 350 cm^{-1} correspond to TO and LO modes, respectively, of wurzite ZnS.[48] LO modes up to sixth order were observed along with clear identification of TO modes up to fifth order. Higher order LO modes are observed owing to Fröhlich interaction originating from strong electron phonon interaction in resonance scattering process.[49] We have estimated electron-LO phonon coupling strength by calculating Huang-Rhys parameter S using the following equation:[50]

$$\left|\frac{I_{2LO}}{I_{1LO}}\right| = \frac{S}{2} \times \frac{(E_{ex} + \hbar\omega_{LO} - \hbar\omega_0)^2 + \Gamma^2}{(E_{ex} + 2\hbar\omega_{LO} - \hbar\omega_0)^2 + \Gamma^2}. \tag{4}$$

The S value is estimated to be ~0.98, which is close to 1 with free exciton binding energy 40 meV,[51] band gap energy 3.7 eV, and the excitonic energy (E_{ex}) in the present study as 3.66 eV [Fig. 6(b)]. The incident photon ($\hbar\omega_o$) and LO phonon ($\hbar\omega_{LO}$) energies are considered to be 3.81 and 0.0434 eV, respectively, along with the exciton linewidth (Γ) of 25 meV,[52] and $I_{2LO}/I_{1LO} = 1.277$. Unusual observation of higher order TO modes including the high intensity in first order mode may be due to strong deformation potential in reduced dimension (few monolayer) of the sample.[53] Figure 6(b) shows the PL spectrum of the nanocomposite using 325 nm excitation at room temperature. The unusual broadening of the PL peak [Fig. 6(b)] around 3.66 eV at room temperature may be due to strong coupling of A, B excitons[51,54] at 3.68 and 3.75 eV with overtones of LO phonon modes. Similar broadening of the PL peak has also been observed for ZnO nanorods where free exciton is reported to couple with overtones of LO phonon.[55] The peak corresponding to the blue shifted band gap value at ~5.4 eV caused by confinement did not appear here, as the excitation energy was limited below it.

Figure 7(a) shows multiphonon Raman scattering for 514.5 nm excitation. The peaks at 175 and 233 cm^{-1} are second order modes belonging to 2TA (transverse acoustic) and 2LA (longitudinal acoustic) phonon modes of wurtzite ZnS at zone boundaries, respectively. Peaks at 290.5 and 368.7 cm^{-1} are blue shifted TO and LO modes belonging to A_1 symmetry of wurtzite ZnS. Excitation dependent shift in the Raman peak positions is well known owing to its sensitivity to electron-phonon coupling as it is observed for 3.81 eV excitation [Fig. 6(a)]. The peak at 315 cm^{-1} may correspond to surface optical (SO) mode. The mode at 441 cm^{-1} can be assigned to a combinational mode frequency of LA+LO of wurtzite ZnS.[56]

Contribution from the non-zone center phonons in nanostructures, with finite crystallite size, corresponding to the discrete allowed wavevectors contribute to the Raman intensity. It leads to Raman lineshape analysis by adding the contribution of each of these modes with their own natural linewidth along with suitable q-dependent weight or intensity factors. A scheme was discussed,[57–59] using a phenomenological approach based on spatial correlation model for the Raman lineshape analysis. The first-order Raman spectrum is calculated by integrating contributions over the complete Brillouin zone, for $\omega(q)$ derived from the phonon dispersion curve and Γ_0 being the natural line width of zone center optical phonon in bulk ZnS.[56] However, in contrast to the phonon confinement model, which predicts a red shift of optical phonon as a function of size of nanoparticle, a blue shift of optical phonon is observed for the optical TO and LO modes at 290.5 and 368.7 cm^{-1}, respectively. The peak positions expected from phonon confinement model for TO and LO mode are 267 and 342 cm^{-1} considering bulk values of 275 and 350 cm^{-1}, respectively.[56,57] The Γ_0 value for the TO and LO modes are taken approximately as 10 and 7.8 cm^{-1}, respectively, along with shift of phonon frequencies at the adjacent zone boundary as 17 cm^{-1} for both the modes from the reported calculated phonon dispersion data for wurtzite ZnS.[56] The blue shift of optical phonon frequencies can arise if the embedded ZnS nanosheets experience compressive stress. During synthesis when the specimen was cooled from 873 K to 303 K, a compressive stress was induced on ZnS phase due to thermal expansion coefficient mismatch between Na-4 mica and ZnS phases. Considering thermal expansion coefficients of Na-4 mica as $80 \times 10^{-6}/K$[60] and of ZnS as $4.6 \times 10^{-6}/K$[61] and bulk modulus of ZnS as 74 GPa,[62] the estimated value of compressive stress was found to be ~3.2 GPa. The pressure exerted by the Na-4 mica on ZnS can be obtained from the blue shift of optical phonon frequency also. The pressure induced shift of phonon frequency in ZnS is given as[63]

$$\omega_{TO} = 267 + 0.62P, \quad \omega_{LO} = 342 + 0.43P,$$

where ω is in cm^{-1} and P in kbar (0.1 GPa). For ω_{TO} and ω_{LO} the pressures are calculated to be approximately 3.8 and 6.2 GPa, respectively. The pressure for ω_{TO} is in good agreement with the stress generated during synthesis, which occurs along the perpendicular direction of the nanosheets. The pressure values are distinctly different while calculating for TO and LO modes. The compressive stress along the perpendicular direction will bring about a lateral deformation along the basal plane of the ZnS nanosheets due to Poisson's ratio of the material. Such deformation will be contributed by the neighboring Na-4 mica grains containing ZnS nanosheets. Thus the total effective stress related to ω_{LO} mode will be enhanced many-fold. Although it is difficult to quantify the value, such stress rationalizes the calculated value of 6.2 GPa.

Regarding the peak at 315 cm^{-1}, SO mode in polar crystals with large intensities is reported in between TO and the corresponding LO mode. The SO mode can be invoked in the presence of surface modulation of nanosheets.[64] The dispersion relations for SO phonons (ω_{SO}) for a ZnS nanoribbon

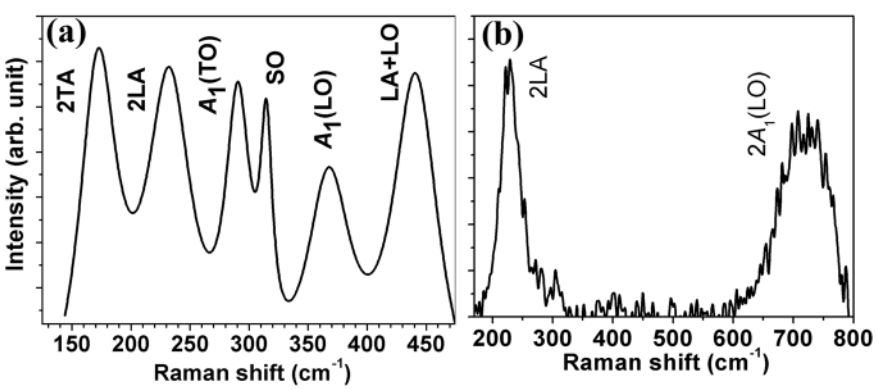

FIG. 7. Multiphonon modes combined of fundamental, surface optical, zone boundary and combination modes in ZnS using (a) Ar^+ laser of 514.5 nm and (b) InGaAs line laser of 785 nm.

is already reported earlier,[65] for the symmetric (S) SO mode and antisymmetric (AS) SO modes for the q_iL_i for the slab, $L_i(i=x,y)$ whose growth direction is along z, and $q_i(i=x,y)$ is the phonon wavevector. Mode frequency value of 315 cm^{-1} corresponds to $q_iL_i/2=0.22$ as per S-SO mode dispersion relation (Fig. 4 of Ref. 65) of ZnS nanoribbons. We can consider our ZnS nanosheet as arranged nanoribbons. If we take the average nanoribbon cross section dimensions to be $\sim 100 \times 0.6$ $(L_x \times L_y)$ nm^2 (considering a monolayer thickness $(L_y) \approx 0.6$ nm), we can then calculate the wavelengths for the surface potential perturbation that breaks the symmetry and activates the SO mode Raman scattering $\lambda_{SO}=2\pi/q_i$ $(i=x,y)$, ~8.6 nm (y ~ 0.6 nm), and ~1427 nm ($x \sim 100$ nm). Surface roughness with a modulation of ~8.6 nm is observed [indicated by arrows in Fig. 3(a)] and any integer multiple equivalent to the λ (fundamental mode ~8.6 nm or $166 \times 8.6\,nm = 1427.6\,nm$) will be sufficient to initiate breakdown of translational symmetry for the contribution of surface potential toward SO modes. One can also see that the intensity of the observed SO phonons in the present study are comparable to other phonons. The magnitude of surface roughness determines the SO peak intensity owing to the breakdown of the translational symmetry of the surface potential.[64]

For the 785 nm excitation (Fig. 7(b)), overtone modes of 2LA and $2A_1$(LO) are observed at 230 and 725 cm^{-1}, respectively. Small discrepancies in the overtone modes as compared to integral multiple of the fundamental mode are due to the reason that the former are not the zone center phonons and thus the deviations are expected.

IV. SUMMARY AND CONCLUSIONS

In summary, ultrathin stable wurtzite ZnS nanosheets are grown within the interlayer spaces of Na-4 mica with a thickness of 0.6 nm by an ion-exchange-cum-solution treatment process followed by sulfidation treatment at relatively low temperature of 873 K. The thickness is confirmed by AFM study. The two-dimensional morphology of ZnS gives a large blue shift of 1.7 eV of the band gap, and the calculated thickness is in reasonable agreement with that estimated from crystallographic consideration of material growth within the interlayer spaces of thickness ~0.6 nm. Raman scattering studies show higher order TO modes caused by deformation potential in reduced dimension. A blue shift of TO and LO modes, rather than red shift in confined phonon, is ascribed to compressive stress on ZnS nanosheets. PL spectrum shows a broadening due to coupling between excitons and LO overtones. This nanocomposite is proposed to have application in UV detection of both bands, viz., UV-A and UV-C.

ACKNOWLEDGMENTS

Support for this work was derived from a grant by the Department of Science and Technology under an Indo-Australian Project on nanocomposites. A. Mandal and S. Mitra thank University Grants Commission, New Delhi for Senior Research Fellowships. D. Chakravorty thanks Indian National Science Academy, New Delhi, for the award of an Honorary Scientist's position.

[1]G. Z. Shen, Y. Bando, and D. Golberg, J. Phys. Chem. B **110**, 20777 (2006).
[2]D. Moore and Z. L. Wang, J. Mater. Chem. **16**, 3898 (2006).
[3]P. Hu, Y. Liu, L. Fu, L. Cao, and D. Zhu, J. Phys. Chem. B **108**, 936 (2004).
[4]N. Tokio, F. Keisuke, and K. Akio, IEEE Trans. Electron. Devices **46**, 2093 (1999).
[5]A. Fujii, H. Wada, K.-i. Shibata *et al*., Proc. SPIE **4375**, 206 (2001).
[6]M. Chattopadhyay, P. Kumbhakar, C. S. Tiwary, and A. K. Mitra, J. Appl. Phys. **105**, 024313 (2009).
[7]M. Chattopadhyay, P. Kumbhakar, R. Sarkar, R. Sarkar, A. K. Mitra, and U. Chatterjee, Appl. Phys. Lett. **95**, 163115 (2009).
[8]Y. Wang and N. J. Herron, Phys. Chem. **95**, 525 (1991).
[9]A. P. Alivisatos, Science **271**, 933 (1996).
[10]W. Chen, Z. Wang, Z. Lin, and L. Lin, Appl. Phys. Lett. **70**(11), 1465 (1997).
[11]R. N. Bhargava, D. Gallagher, X. Hong, and A. Nurmikko, Phys. Rev. Lett. **72**, 416 (1994).
[12]K. Sooklal, B. S. Cullum, S. M. Angel, and C. J. Murphy, J. Phys. Chem. **100**, 4551 (1996).
[13]N. Murase, R. Jagannathan, Y. Kanematsu, M. Watanabe, A. Kurita, K. Hirata, T. Yazawa, and T. Kushida, J. Phys. Chem. B **103**, 754 (1999).
[14]Y. Li, Y. Ding, Y. Zhang, and Y. Qian, J. Phys. Chem. Solids **60**, 13 (1999).
[15]S. Song and Q. Gao, J. Appl. Phys. **99**, 106107 (2006).
[16]S. Sapra, A. Prakash, A. Ghangrekar, N. Periasamy, and D. D. Sarma, J. Phys. Chem. B **109**, 1663 (2005).
[17]G. C. Trigunyat and G. K. Chadha, Phys. Status Solidi A **4**, 9 (1971).
[18]Y. Zhao, Y. Zhang, H. Zhu, G. C. Hadjipanayis, and J. Q. Xiao, J. Am. Chem. Soc. **126**, 6874 (2004).
[19]S. H. Yu and M. Yoshimura, Adv. Mater. **14**, 296 (2002).
[20]S. B. Qadri, E. F. Skelton, D. Hsu, A. D. Dinsmore, J. Yang, H. F. Gray, and B. R. Ratna, Phys. Rev. B **60**, 9191 (1999).
[21]Z. W. Pan, Z. R. Dai, and Z. L. Wang, Science **291**, 1947 (2001).
[22]Y. W. Wang, L. D. Zhang, C. H. Liang, G. Z. Wang, and X. S. Peng, Chem. Phys. Lett. **357**, 314 (2002).
[23]X. S. Fang and L. D. Zhang, J. Mater. Sci. Technol. **22**, 721 (2006).
[24]Y. Jiang, W. J. Zhang, J. S. Jie, X. M. Meng, J. A. Zapien, and S. T. Lee, Adv. Mater. **18**, 1527 (2006).
[25]C. Ma, M. Moore, J. Li, and Z. L. Wang, Adv. Mater. **15**, 228 (2003).
[26]S. Kar and S. Chaudhuri, J. Phys. Chem. B **109**, 3298 (2005).
[27]L. W. Yin, Y. Bando, J. H. Zhan, M. S. Li, and D. Goldberg, Adv. Mater. **17**, 1972 (2005).
[28]X. S. Fang, C. H. Ye, L. D. Zhang, Y. H. Wang, and Y. C. Wu, Adv. Funct. Mater. **15**, 63 (2005).
[29]J. Zhang, Y. D. Yang, F. H. Jiang, J. P. Li, B. L. Xu, X. C. Wang, and S. M. Wang, Nanotechnol. **17**, 2695 (2006).
[30]C. H. Liang, Y. Shimizu, T. Sasaki, H. Umehara, and N. Koshizaki, J. Phys. Chem. B **108**, 9728 (2004).
[31]Z.-X. Deng, C. Wang, X.-M. Sun, and Y.-D. Li, Inorg. Chem. **41**, 869 (2002).
[32]X.-S. Fang, C.-H. Ye, X.-S. Peng, Y.-H. Wang, Y.-C. Wu, and L.-D. Zhang, J. Cryst. Growth **263**, 263 (2004).
[33]G. H. Yue, P. X. Yan, D. Yan, J. Z. Liu, D. M. Qu, Q. Yang, and X. Y. Fan, J. Cryst. Growth **293**, 428 (2006).
[34]S. Bhattacharya, A. Datta, S. Dhara, and D. Chakravorty, J. Phys. D: Appl. Phys. **42**, 235504 (2009).
[35]S. Mitra, A. Mandal, A. Datta, S. Banerjee, and D. Chakravorty, Euro. Phys. Lett. **92**, 26003 (2010).
[36]S. Mitra, A. Mandal, A. Datta, S. Banerjee, and D. Chakravorty, J. Phys. Chem. C **115**, 14673 (2011).
[37]W. J. Paulus, S. Komarneni, and R. Roy, Nature (London) **357**, 571 (1992).
[38]T. Kodama and S. Komarneni, J. Mater. Chem. **9**, 533 (1999).
[39]M. Park, D. H. Lee, C. L. Choi, S. S. Kim, K. S. Kim, and J. Choi, Chem. Mater. **14**, 2582 (2002).
[40]A. D. Yoffe, Adv. Phys. **42**, 173 (1993).
[41]C. Schliehe, B. H. Juarez, M. Pelletier, S. Jander, D. Greshnykh, M. Nagel, A. Meyer, S. Foerster, A. Kornowski, C. Klinke, and H. Weller, Science **329**, 550 (2010).

[42]X. Fang, Y. Bando, C. Ye, G. Shen, and D. Golberg, J. Phys. Chem. C **111**, 8469 (2007).
[43]R. Sarkar, C. S. Tiwary, P. Kumbhakar, S. Basu, and A. K. Mitra, Physica E **40**, 3115 (2008).
[44]C. S. Tiwary, P. Kumbhakar, A. K. Mondal, and A. K. Mitra, Phys. Status Solidi A **207**, 1874 (2010).
[45]F. Consadori and R. F. Frindt, Phys. Rev. B **2**, 4893 (1970).
[46]P. E. Lippens and M. Lannoo, Phys. Rev. B **39**, 10935 (1989).
[47]S. Bhattacharya, A. Datta, S. Dhara, and D. Chakravorty, J. Raman Spectrosc. **42**, 429 (2011).
[48]R. Marshall and S. S. Mitra, Phys. Rev. **134**, A1019 (1964).
[49]S. Dhara, S. Chandra, G. Mangamma, S. Kalavathi, P. Shankar, K. G. M. Nair, A. K. Tyagi, C. W. Hsu, C. C. Kuo, L. C. Chen, K. H. Chen, and K. K. Sriram, Appl. Phys. Lett. **90**, 213104 (2007).
[50]Q. Zhang, J. Zhang, M. I. B. Utama, B. Peng, M. de la Mata, J. Arbiol, and Q. Xiong, Phys. Rev. B **85**, 085418 (2012).
[51]Q. Xiong, G. Chen, J. D. Acord, X. Liu, J. J. Zengel, H. R. Gutierrez, J. M. Redwing, L. C. L. Y. Voon, B. Lassen, and P. C. Eklund, Nano Lett. **4**, 1663 (2004).
[52]H. C. Ong and R. P. H. Chang, Appl. Phys. Lett. **79**, 3612 (2001).
[53]R. L. Schmidt, K. Kunc, M. Cardona, and H. Bilz, Phys. Rev. B **20**, 3345 (1979).
[54]R. Chen, D. Li, B. Liu, Z. Peng, G. G. Gurzadyan, Q. Xiong, and H. Sun, Nano Lett **10**, 4956 (2010).
[55]S. Chakraborty, S. Dhara, T. R. Ravindran, S. S. Pal, M. Kamruddin, and A. K. Tyagi, AIP Adv. **1**, 032135 (2011).
[56]Y. C. Cheng, C. Q. Jin, F. Gao, X. L. Wu, W. Zhong, S. H. Li, and P. K. Chu, J. Appl. Phys. **106**, 123505 (2009).
[57]S. Sahoo, S. Dhara, S. Mahadevan, and A. K. Arora, J. Nanosci. Nanotechnol. **9**, 5604 (2009).
[58]K. W. Adu, H. R. Gutiérrez, U. J. Kim, G. U. Sumanasekera, and P. C. Eklund, Nano Lett. **5**, 409 (2005).
[59]K. W. Adu, Q. Xiong, H. R. Gutiérrez, G. Chen, and P. C. Eklund, Appl. Phys. A **85**, 287–297 (2006).
[60]A. Mandal, A. Bose, S. Mitra, A. Datta, S. Banerjee, and D. Chakravorty, J. Magn. Magn. Mater. **324**, 2861 (2012).
[61]R. R. Reeber and G. W. Powell, J. Appl. Phys. **38**, 1531 (1967).
[62]K. Wright and J. D. Gale, Phys. Rev. B **70**, 035211 (2004).
[63]Y. Ebisuzaki and M. Nicol, J. Phys. Chem. Solids **33**, 763 (1971).
[64]S. Dhara, P. Sahoo, A. K. Tyagi, and B. Raj "Surface optical modes in semiconductor nanowire" in *Nanowires-Implementation and Applications*, edited by A. Hashim (Intech Open Access, Croatia, 2011).
[65]Q. Xiong, J. Wang, O. Reese, L. C. Yoon, and P. C. Eklund, Nano Lett. **4**, 1991 (2004).